Efficiency of nonspinning templates in gravitational wave searches for aligned-spin binary black holes

Hee-Suk Cho*
Korea Institute of Science and Technology Information, Daejeon 305-806, Korea
(Dated: September 21, 2016)

We study the efficiency of nonspinning waveform templates in gravitational wave searches for aligned-spin binary black holes (BBHs). We use PhenomD, which is the most recent phenomenological waveform model designed to generate the full inspiral-merger-ringdown waveforms emitted from BBHs with the spins aligned with the orbital angular momentum. Here, we treat the effect of aligned-spins with a single spin parameter χ. We consider the BBH signals with moderately small spins in the range of $-0.4 \leq \chi \leq 0.4$. Using nonspinning templates, we calculate fitting factors of the aligned-spin signals in a wide mass range up to $\sim 100M_{\odot}$. We find that the signals with negative spins can have higher fitting factors than those with positive spins. If $\chi = 0.3$, only the highly asymmetric-mass signals can have the fitting factors exceeding the threshold of 0.965, while the fitting factors for all of the signals can be larger than the threshold if $\chi = -0.3$. We demonstrate that the discrepancy between the regions of a positive and a negative spins is due to the physical boundary ($\eta \leq 0.25$) of the template parameter space. We also show that the recovered mass parameters can be significantly biased from the true parameters. We examine the impact of the systematic bias on the parameter estimation by comparing the bias with the statistical error.

PACS numbers: 04.30.–w, 04.80.Nn, 95.55.Ym

arXiv:1609.06039v1 [gr-qc] 20 Sep 2016

I. INTRODUCTION

Recently, two gravitational wave (GW) signals, named as GW150914 and GW151226, were detected by the two LIGO detectors [1, 2], and these observations indicate that future observing runs of the advanced detector network [3–5] will yield more binary black hole (BBH) merger signals [6–9]. Detailed analyses in the parameter estimation showed that both signals were emitted from merging BBHs [2, 10, 11]. The masses of the two binaries were found to be ~ 65 and $22M_{\odot}$ for GW150914 and GW151226, respectively. In particular, the two components of GW150914 are the heaviest stellar mass BHs known to date. On the other hand, the precession effects for both signals were poorly measured, while the aligned-spins (χ) were meaningfully constrained. Although we might expect high-spin BHs from the X-ray observations [12], both binaries had small values of χ. The 90% credible intervals in their parameter estimations were in the range of $-0.4 \leq \chi \leq 0.4$.

The waveforms emitted from BBHs have three phases: inspiral, merger, and ringdwon (IMR), and the IMR phases of stellar mass BBHs are likely to be captured in the sensitivity band of ground-based detectors. In the search for BBHs, therefore, we have to use the full IMR waveforms as templates. Over the past decade, two classes of IMR waveform models have been developed: the effective-one-body calibrated to numerical relativity simulations (EOBNR) and the phenomenological models. Since EOBNR is formulated in the time domain as a set of differential equations, generation of those waveforms are computationally much more expensive than generation of frequency-domain waveforms. Therefore, for the purpose of the GW data analysis, Pürrer [13, 14] has recently built a Fourier-domain reduced order model that faithfully represents the original EOBNR model [15, 16]. On the other hand, a series of the phenomenological models have been developed, and those were also constructed in the frequency domain. The first phenomenological model was PhenomA [17–19] that was designed to model the IMR waveforms of nonspinning BBHs, and this model was extended to an aligned-spin system in PhenomB [20] by adding the effective spin parameter χ. The third model was PhenomC [21] that was also designed for aligned-spin BBHs, and extended to a precessing system in PhenomP [22]. The most recent phenomenological model is PhenomD [23]. This model is also designed for aligned-spin BBHs but covers much wider ranges of mass (up to mass ratios of $1:18$) and spin (up to $|\chi| \sim 0.85$) than any other phenomenological models. Recently, it has been shown that PhenomD can perform very well for BBH searches, losing less than 1% of the recoverable signal-to-noise ratio [24]. Therefore, we exploit PhenomD for the waveforms of aligned-spin BBHs in this work[1].

We study the efficiency of nonspinning waveform templates in GW searches for aligned-spin BBH signals by investigating the fitting factor. Similar works have been carried by several authors in the past few years. Using the post-Newtonian waveform model, Ajith [25] calculated fitting factors for several binaries with masses of $M \leq 20M_{\odot}$. He found that the spin value of the signal clearly separated the population of binaries producing a poor fitting factor from those producing a high fitting factor (see Fig. 11 therein). Dal Canton *et al.*[26] also calculated fitting factors for BH-neutron star (NS) binaries with masses of $M \leq 18M_{\odot}$, and they also found a clear separation between the two populations (see

*Electronic address: chohs1439@pusan.ac.kr

[1] The recent version of EOBNR reduced order model was also calibrated in wide parameter ranges up to mass ratios of $1:100$ and spins of $-1 \leq \chi_i \leq 0.99$ [14].

Fig. 8 therein). In the same paper, the authors showed that this behavior was due to the fact that the template parameter space is physically bounded as $\eta \leq 0.25$ (see Figs. 5 and 6 therein). A similar work has also been performed by Privitera *et al.*[27] for BBH systems with $10M_\odot \leq M \leq 30M_\odot$ and $m_1/m_2 \leq 4$ using the PhenomB waveforms [20]. They found that a nonspinning template bank achieved fitting factors exceeding 0.97 over a wide region of parameter space, spanning roughly $-0.25 \leq \chi \leq 0.25$ over the entire mass range considered in their work (see Fig. 1 therein). Recently, the work of [27] has been extended to higher mass systems $M \leq 50M_\odot$ by Capano *et al.*[28] using the EOBNR waveforms [16]. On the other hand, several works have used precessing signals to test a nonspinning and an aligned-spin template banks [29–32].

In this work, we revisit the issues on the effectualness of nonspinning templates for aligned-spin BBH signals. While the works of [27, 28] have focused on the effectual aligned-spin template banks and their gains in searches for aligned-spin BBHs in a wide spin range, we focus our attention on the signals with moderately small spins in the range of $-0.4 \leq \chi \leq 0.4$. In addition, although the template bank used for current Advanced LIGO searches covers the binary masses up to $100M_\odot$ [33, 34], the previous works have only considered low-mass systems. Here, we extend the study to high-mass systems up to $M = 100M_\odot$. We also show the systematic bias and examine the validity of nonspinning templates for the parameter estimation.

II. GW DATA ANALYSIS

A. BBH search

In signal processing, if a signal of know shape is buried in stationary Gaussian noise, the matched filter can be the optimal method to identify the signal. For the GWs emitted from merging BBHs, since there exist various models that can produce accurate full IMR waveforms, the matched filter can be employed in the BBH searches. If a detector data stream $x(t)$ contains stationary Gaussian noise $n(t)$ and a GW signal $s(t)$, the match between $x(t)$ and a template waveform $h(t)$ is determined by

$$\langle x|h\rangle = 4\mathrm{Re}\int_{f_{\rm low}}^{\infty} \frac{\tilde{x}(f)\tilde{h}^*(f)}{S_n(f)}df, \tag{1}$$

where the tilde denotes the Fourier transform of the time-domain waveform, $S_n(f)$ is the power spectral density (PSD) of the detector noise, and $f_{\rm low}$ is the low frequency cutoff that depends on the shape of $S_n(f)$. In this work, we consider a single detector configuration and use the zero-detuned, high-power noise PSD with $f_{\rm low} = 10$ Hz [35]. Using the relation in Eq. (1), the signal-to-noise ratio ρ (SNR) can be determined by

$$\rho = \langle s|\hat{h}\rangle, \tag{2}$$

where $\hat{h} \equiv h/\langle h|h\rangle^{1/2}$ is the normalized template. When the template waveform h has the same shape as the signal waveform s, the matched filter gives the optimal SNR as

$$\rho_{\rm opt} = \langle s|s\rangle^{1/2}. \tag{3}$$

If the template has a different shape, the SNR is reduced to

$$\rho = \mathrm{FF} \times \rho_{\rm opt}, \tag{4}$$

where FF is the fitting factor defined as the best-match between a normalized signal and a set of normalized templates [36]. For the GW data analysis purposes, the fitting factor is considered to evaluate the search efficiency. Since the detection rate is proportional to $\rho^{1/3}$, a $\mathrm{FF} \simeq 0.97$ corresponds to a loss of detection rates of $\sim 10\%$.

To fully describe the wave function of an aligned-spin BBH system, we need 11 parameters except the eccentricity. Those are five extrinsic parameters (luminosity distance of the binary, two angles defining the sky position of the binary with respect to the detector, orbital inclination, and wave polarization), four intrinsic parameters (component masses and spins), the coalescence time t_c, and the coalescence phase ϕ_c. However, since the extrinsic parameters only scale the wave amplitude, and we work with the normalized wave function, we do not need to consider the extrinsic parameters in our analysis. In addition, the inverse Fourier transform of the match can give the output for all possible coalescence times at once, and we can maximize the match over all possible coalescence phases by taking the absolute value of the complex-valued output (see [37] for more details). Therefore, we need only the intrinsic parameters $(m_1, m_2, \chi_1, \chi_2)$ in our analysis, and those are the input parameters of PhenomD.

On the other hand, it is often more efficient to treat the effect of aligned-spins with a single spin parameter rather than the two component spins because the two spins are strongly correlated [38]. For this purpose, the spin effects in the phenomenological models are parameterized by a effective spin χ:

$$\chi \equiv \frac{m_1\chi_1 + m_2\chi_2}{M}. \tag{5}$$

The value of χ can be determined simply by choosing $\chi_1 = \chi_2 = \chi$ in the PhenomD wave function[2]. Thus, our signal waveform is given by $h_s = h(m_1, m_2, \chi) = h_{\rm PhenomD}(m_1, m_2, \chi, \chi)$, while the nonspinning templates are given by $h_t = h(m_1, m_2) = h_{\rm PhenomD}(m_1, m_2, 0, 0)$.

In this work, we define the overlap P by the match between the signal $\hat{h}_s$ and the template $\hat{h}_t$ maximized over t_c and ϕ_c:

$$P = \max_{t_c,\phi_c}\langle \hat{h}_s|\hat{h}_t\rangle. \tag{6}$$

Thus, we can have $P = 1$ if the signal and the template have the same shapes. Changing the mass parameters of the nonspinning templates, we calculate the two-dimensional overlap

[2] PhenomD is parameterized by a normalized reduced effective spin $\hat{\chi}$ [23], but we can have $\hat{\chi} = \chi$ by choosing $\chi_1 = \chi_2$.

surface as

$$P(\lambda) = \max_{t_c,\phi_c} \langle \hat{h}_s(\lambda_0) | \hat{h}_t(\lambda) \rangle, \tag{7}$$

where λ_0 denotes the true values of the mass and the spin of the signal, and λ denotes the mass parameters of the template. Then, in our analysis the fitting factor corresponds to the maximum value in the overlap surface:

$$\mathrm{FF} = \max_{\lambda} P(\lambda). \tag{8}$$

On the other hand, in an actual search for BBHs the template waveforms are discretely placed in the bank, hence the fitting factor can be marginally reduced depending on the template density. Thus, the effective fitting factor is obtained by

$$\mathrm{FF}_{\mathrm{eff}} = \max_{h_t \in \mathrm{bank}} P(\lambda). \tag{9}$$

Typically, when one chooses a waveform model for the search, the template bank is constructed densely enough such that the mismatch between the templates and the signal does not exceed 3% including the effect of the discreteness of the template spacing, i.e. $1 - \mathrm{FF}_{\mathrm{eff}} \geq 0.97$ [39, 40]. In this work, however, we want to remove the effect of discreteness on the fitting factor. To do so, we choose sufficiently fine spacings in the template space defined in the $M_c - \eta$ plane [41, 42].[3] For example, in order to obtain $\mathrm{FF}_{\mathrm{eff}}$ for one signal, we repeat a grid search around λ_0 until we find the crude location of the peak point in the overlap surface. Next, we estimate the size of the contour $\bar{P} \equiv P/P_{\max} = 0.995$, where $P_{\max}$ is the maximum overlap value in that contour (if the recovered mass parameters are biased from λ_0, then $P_{\max} < 1$), hence $\bar{P}$ corresponds to the weighted overlap. Finally, we find (almost) the exact location of the peak point by performing a 31×31 grid search in the region of $\bar{P} > 0.995$, and the overlap value at the peak point is regarded as FF.

Once a fitting factor is determined through the above procedure, we can measure the systematic bias, which corresponds to the distance from the true value λ_0 to the recovered value λ^{rec}:

$$b = \lambda^{\mathrm{rec}} - \lambda_0. \tag{10}$$

Typically, the recovered parameters are systematically biased from the true parameters if the incomplete template waveforms are used. In our analysis, the incompleteness of templates arises from neglecting the spin effect in the wave function. As the efficiency of a template waveform model for the search is evaluated by the fitting factor, its validity for the parameter estimation can be examined by the systematic bias. The impact of the bias on the parameter estimation can be measured by comparing that with the statistical error. In the following subsection, we briefly describe how the statistical error can be calculated from the overlap surface.

[3] In general, the overlap surface is obtained more efficiently in the parameter space consisting of the chirp mass ($M_c \equiv (m_1 m_2)^{3/5}/M^{1/5}$) and the symmetric mass ratio ($\eta \equiv m_1 m_2/M^2$), so we take into account the parameters M_c, η instead of m_1, m_2 in the overlap calculations.

B. Parameter estimation

Once a detection is made in the search pipeline, the parameter estimation pipeline conducts post-processing with the data stream, that contains the GW signal, to figure out the physical property of the binary source [43]. The parameter estimation analysis employs Bayesian approach. Using the match formalism defined in Eq. (1), the posterior probability, that the GW signal in the data stream x is characterized by the parameters λ, can be expressed by

$$p(\lambda|x) \propto p(\lambda) L(x|\lambda), \tag{11}$$

where $p(\lambda)$ is the prior probability and $L(x|\lambda)$ is the likelihood, which can be written as [44, 45]

$$L(x|\lambda) \propto \exp\left[-\frac{1}{2} \langle x - h(\lambda) | x - h(\lambda) \rangle \right], \tag{12}$$

with $h(\lambda)$ being a template waveform. In the parameter estimation, the extrinsic parameters as well as t_c and ϕ_c are also considered as the variables for λ. In this case, an extremely large number of waveforms is necessary to construct a template bank because the bank has to cover a high-dimensional parameter space. Thus, in the parameter estimation, rather than the bank-based analysis, the templates are generated sequentially by changing the parameter values until the algorithm recovers the true parameters. The results of the parameter estimation are given by the posterior probability density functions (PDFs) for the parameters [43].

In Eq. (11), if we assume a flat prior, the posterior PDF is determined by the likelihood. In the high SNR limit, the likelihood function obeys a Gaussian distribution, and the log likelihood can be approximated by the overlap as [46]

$$\ln L(\lambda) = -\rho^2 (1 - P(\lambda)). \tag{13}$$

From this relation, we can infer that the confidence region of the posterior PDF is associated with a certain region in the overlap surface. We can also predict that the overlap surface has a quadratic shape in the confidence region because the likelihood function is Gaussian. The connection between the confidence region and the overlap surface has been given by Baird *et al.* [47]. They showed that the confidence region is approximately consistent with the overlap region that is surrounded by the iso-match contour (IMC) determined by

$$P = 1 - \frac{\chi_k^2 (1-p)}{2\rho^2}, \tag{14}$$

where $\chi_k^2(1-p)$ is the chi-square value for which there is $1-p$ probability of obtaining that value or larger, and k denotes the degree of freedom, given by the number of parameters. In this work, since we explore two-dimensional mass parameter space (i.e., $k = 2$), the one-sigma confidence region (i.e., $p = 0.682$) for $\rho = 20$ is given by the contour $P = 0.99714$. On the other hand, the statistical error (σ) for each parameter is given by the confidence interval determined by $P = 0.99876$ in the one-dimensional overlap distribution.

In this work, the one-dimensional overlap distribution can be obtained by marginalizing the original two-dimensional overlap distribution (for more details refer to [48]).[4]

III. RESULT

We choose as our target signals aligned-spin BBHs in the parameter regions of $m_1, m_2 \geq 5M_\odot$ $(m_2 \leq m_1)$, $M \leq 100M_\odot$ and $-0.4 \leq \chi \leq 0.4$. The signal waveforms are generated by using PhenomD with $\chi_1 = \chi_2 = \chi$. We construct a template bank in the $M_c - \eta$ plane with nonspinning waveforms assuming $\chi_1 = \chi_2 = 0$ in PhenomD. The templates are assumed to be placed densely enough so that we can avoid the effect of the discreteness of the bank. Using the nonspinning templates with an aligned-spin signal we calculate the overlap surface that includes the confidence region, and determine the fitting factor and the systematic bias for the signal.

A. Fitting factor

In Fig. 1, we show the fitting factors for all of the BBH signals. In each panel, the darkest region corresponds to the signals that cannot achieve the fitting factor exceeding a threshold of 0.965 beyond which a loss of detection rates does not exceed $\sim 10\%$. We find that the signals with negative spins can have higher fitting factors than those with positive spins. If $\chi = 0.3$, only the highly asymmetric-mass signals can have the fitting factors exceeding the threshold. However, if $\chi = -0.3$, the fitting factors for all of the signals can be larger than the threshold, and if $\chi = -0.4$, about two third of the signals can have fitting factors exceeding the threshold. In particular, if the signal has a small spin in the range of $-0.1 \leq \chi \leq 0.1$, the fitting factor can be larger than 0.99 (the lightest region) for all of the signals except those in the highly symmetric-mass region. Only few signals among our binaries can achieve $\mathrm{FF} \geq 0.965$ in the spin range of $-0.4 \leq \chi \leq 0.4$, and we show several examples in Fig. 2.

In Fig. 3, we also show the fitting factors in the $M-\eta$ plane using the same color scales as in Fig. 1. In this figure, we can interpret the pattern of the fitting factors more easily. In the region of a negative spin, the fitting factor tends to decrease as the total mass or the symmetric mass ratio increases. On the other hand, in the region of a positive spin, we can see a strong dependence of the fitting factor on the symmetric mass ratio. In this case, the fitting factors in the symmetric-mass region rapidly decrease with increasing χ, especially, those with low masses can drop below the threshold even with the small spin of $\chi = 0.1$. In Fig. 4a, we show some examples that show highly asymmetric fitting factors between a positive and a negative spins. We find that if $\chi > 0$, the fitting factor suddenly falls off at a certain spin value, and the falling rate tends to slacken for higher masses.

Dal Canton *et al.*[26] showed that the sudden fall-off of the fitting factor is associated with the physical boundary of the template space. For the (positively) aligned-spin signals, the parameter value of η recovered by the nonspinning templates increases as the spin of the signal increases. However, in the parameter space of (M_c, η), the physical value of η should be restricted to the range of $0 \leq \eta \leq 0.25$. Thus, the recovered value of η cannot exceed 0.25 even though the signal has higher spins. For example, Fig. 4b shows the recovered η (η^{rec}) as a function of χ for the same binaries as in Fig. 4a. If the true value of η is 0.25, η^{rec} is already at the boundary at $\chi = 0$, hence always equal to 0.25 in the entire range of positive spins. In Fig. 4, we find that the spin value at which the η^{rec} reaches 0.25 is consistent with the one at which the sudden fall-off of the fitting factor occurs. On the other hand, the post-Newtonian waveforms are well behaved for $0 < \eta < 1.0$ although the unphysical value of η implies complex-valued masses. Boyle *et al.*[49] showed that the fitting factors for high-mass systems above $\sim 30M_\odot$ can be significantly improved if η is allowed to range over unphysical values. However, such the unphysical masses are not permitted in the phenomenological models.

B. Comparing with other works

In Fig. 5, we represent the fitting factors in the $\eta-\chi$ plane in a different way. We classify our binaries into low-mass ($M \leq 50M_\odot$), medium-mass ($50M_\odot \leq M \leq 80M_\odot$), and high-mass ($80M_\odot \leq M$) systems, and calculate the mean fitting factors ($\overline{\mathrm{FF}}$) by averaging over M for each system. Note that since we assume the minimum mass of m_2 to be $5M_\odot$, the values of η start from 0.09 (top), ~ 0.06 (bottom left), and ~ 0.05 (bottom right), respectively. We find that the range of χ, in which $\overline{\mathrm{FF}} \geq 0.99$, becomes smaller as η increases, and the overall area with high fitting factors is narrower for higher mass systems. In particular for the low-mass systems, the fitting factor curves in the region of a positive spin rapidly drop to zero. Dal Canton *et al.*[26] also described the fitting factors in the same manner for BH-NS binaries with masses of $M \leq 18M_\odot$ (see Fig. 8 therein), and our result for the low-mass system shows the pattern of fitting factor similar to their result in the region of a positive spin. However, in the region of a negative spin, they had poor fitting factors, and they pointed out that this is because the minimum NS mass in the template bank is limited to $1M_\odot$.

We also describe the fitting factors in the $M - \chi$ plane in Fig. 6 and compare those with the result of Privitera *et al.*[27]. While Privitera *et al.*considered low-mass BBHs in the range of $M \leq 35M_\odot$ with the initial LIGO PSD [50] assuming $f_{\mathrm{low}} = 40$ Hz, we take into account the higher-mass binaries in the range of $M \geq 30M_\odot$[5] with the Advanced LIGO PSD

[4] Since the overlap surface has a quadratic shape and the confidence interval is proportional to ρ^{-2}, we can obtain the relation $\sigma \propto \rho^{-1}$.

[5] Since we have only few samples in the range of $M < 30M_\odot$, we do not

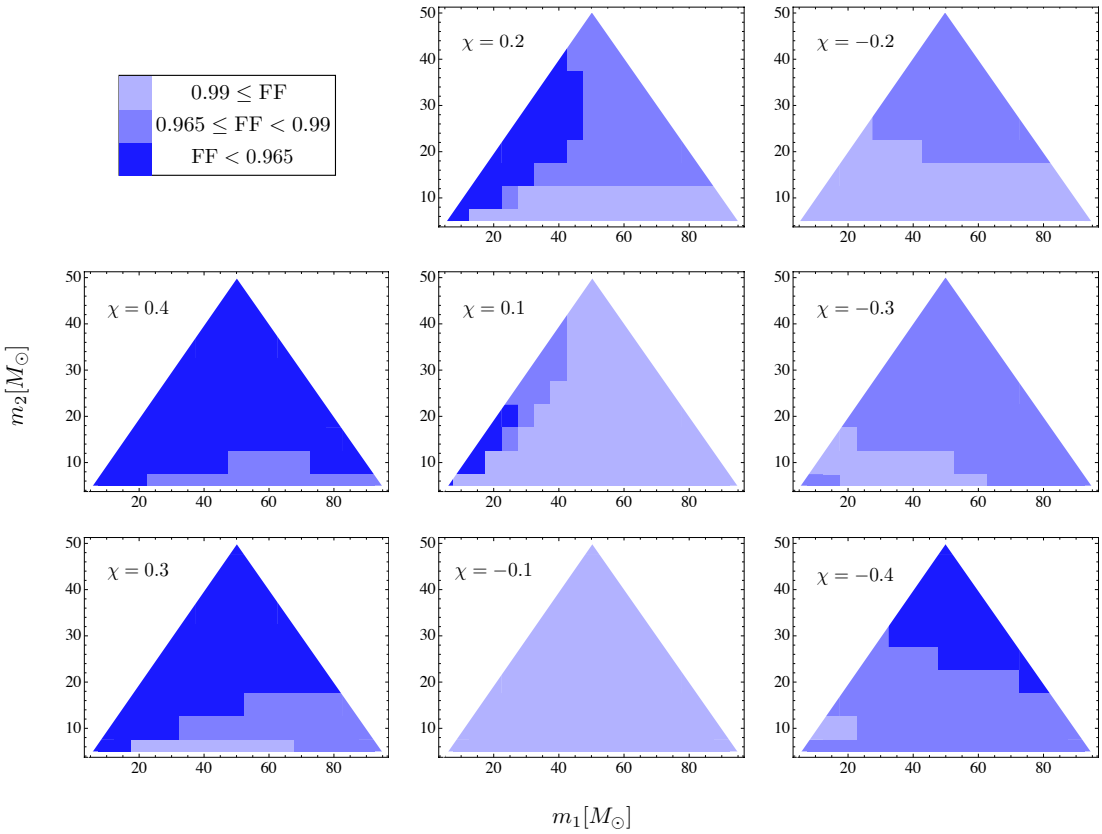

FIG. 1: Fitting factors obtained by using nonspinning templates for aligned-spin BBH signals. The spin value of the signal is given in each panel. The signals with negative spins can have higher fitting factors than those with positive spins

[35] assuming $f_{\rm low} = 10$ Hz. Therefore, our result cannot be directly compared with their result. However, we find that the overall pattern of the fitting factors in our result is similar to the result of [27] (see, Fig. 1 (a) therein). The top panel in Fig. 6 shows very asymmetric fitting factors between the regions of a positive and a negative spins. For positive spins, the fitting factor contours gradually increase as the total mass increases, and this is roughly consistent with the result of [27]. On the contrary, for negative spins, the range of χ, in which the signals have high fitting factors, is much larger than the case for positive spins in the low-mass region, but that becomes smaller as the total mass increases. We already showed that the discrepancy between the two spin regions is caused by the physical boundary of the template space. To see this concretely, we select only the symmetric-mass binaries with $m_1/m_2 \leq 2$ and show their results in the bottom left panel in Fig. 6. We find that the discrepancy is more pronounced compared to the result of the top panel. We also choose the asymmetric-mass binaries for which $\eta^{\rm rec}$ does not reach the physical boundary, i.e., $\eta_{\rm rec} < 0.25$, and show their results in the bottom right panel. As expected, we can see

include the results for those binaries in this figure.

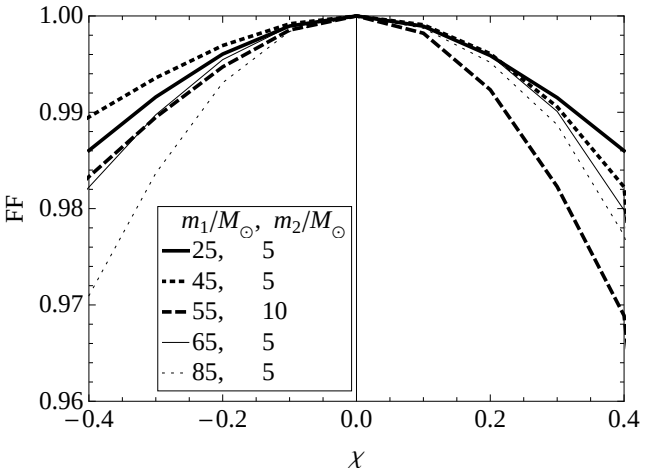

FIG. 2: Examples that have the fitting factors larger than 0.965 in the spin range of $-0.4 \leq \chi \leq 0.4$.

nearly symmetric fitting factors between the regions of a positive and a negative spins. Especially, in this case, most of the binaries can have mean fitting factors greater than 0.965. That means, in the nonspinning template search for aligned-

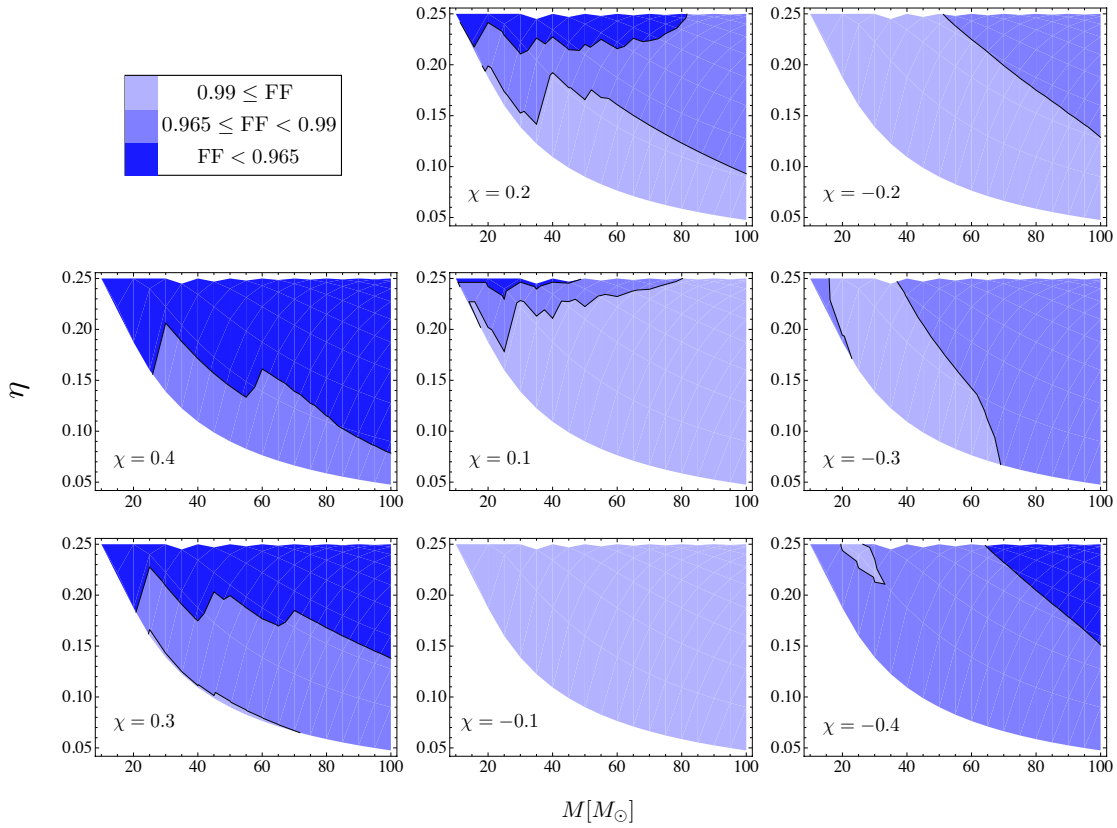

FIG. 3: The same fitting factors as in Fig. 1 but described in the $M-\eta$ plane.

spin BBH signals, most of the signals, that have the masses of $M \leq 100M_{\odot}$ and the spins of $-0.4 \leq \chi \leq 0.4$, have high fitting factors exceeding the threshold 0.965 if only the binary has the asymmetric masses such that $\eta^{\rm rec}$ does not reach 0.25.

C. Systematic bias of the recovered parameter

The purpose of the parameter estimation analysis is to extract the parameters of a signal with high accuracy [40]. However, these algorithms are computationally intensive. On the other hand, in the search, parameters of a signal can also be inferred from the identified template parameters, but the recovered parameters can be significantly biased from the true parameters. In this subsection, we show how much the recovered parameter is biased depending on the spin of the signal.

In Fig. 7, we show the fractional bias (b_λ/λ) as a function of χ. Here, as concrete examples we select several asymmetric-mass binaries that satisfy $\eta^{\rm rec} < 0.25$. In the top panel, as χ increases the bias for η also increases, and the dependence of the bias on χ is stronger for a positive spin than a negative spin. On the contrary, in the bottom left panel, the bias for M_c decreases with increasing χ, and that exhibits a similar dependence on χ between a positive and a negative spins. The biases incorporated in the two mass parameters can be well understood by describing those in terms of a total mass. When the spin is positively aligned with the orbital angular momentum, the spin-orbit coupling makes the binary's phase evolution slightly slower, hence delays the onset of the plunge phase, as compared to its nonspinning counterpart [51]. On the contrary, in the anti-aligned case, the phase evolution becomes slightly faster, and the plunge is hastened. Consequently, for a given starting GW frequency, a positively (negatively) aligned-spin increases (decreases) the length of the waveform, as compared to the nonspinning case. Therefore, positively (negatively) spinning systems can be recovered by lower (higher) mass nonspinning templates. We clearly describe this in the bottom right panel, showing the bias for the parameter M as a function of χ. Interestingly, we find that the systematic bias for M almost linearly depends on χ in our spin range. In addition, all of the results seem to have similar fractional biases (b_M/M) for a given χ even though their masses are very different.

In Fig. 8, we show the fractional biases ($\mathcal{B} \equiv b_M/M$) for the signals with the spins of $\chi = -0.4, -0.2, 0.2$, and 0.4. The red color indicates a negative bias while the blue color indicates a positive bias. We find that the magnitudes of biases are similar between the red and the blue in the asymmetric-mass region ($\eta \lesssim 0.15$), while those are smaller for the positive spins in the symmetric-mass region ($\eta \gtrsim 0.15$). As expected, the difference in the symmetric-mass region is due to the fact that for the positive spins $\eta^{\rm rec}$ is restricted by the

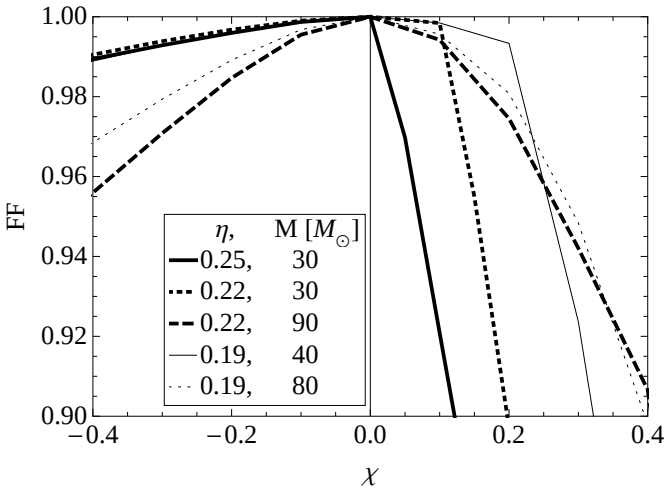

(a) Fitting factor.

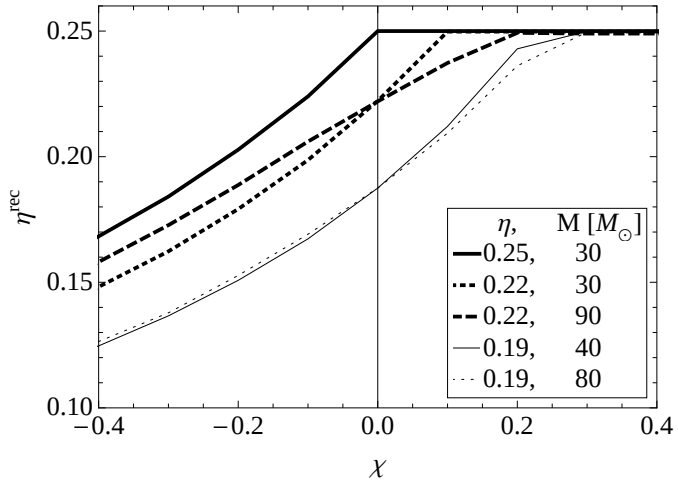

(b) Recovered η.

FIG. 4: Fitting factors and recovered η ($\eta^{\rm rec}$) for several binaries. When $\chi > 0$, the fitting factor suddenly falls off at a certain spin value (a). $\eta^{\rm rec}$ cannot exceed the physical boundary 0.25 (b). The spin value at which $\eta^{\rm rec}$ reaches 0.25 is consistent with the one at which the sudden fall-off of the fitting factor occurs.

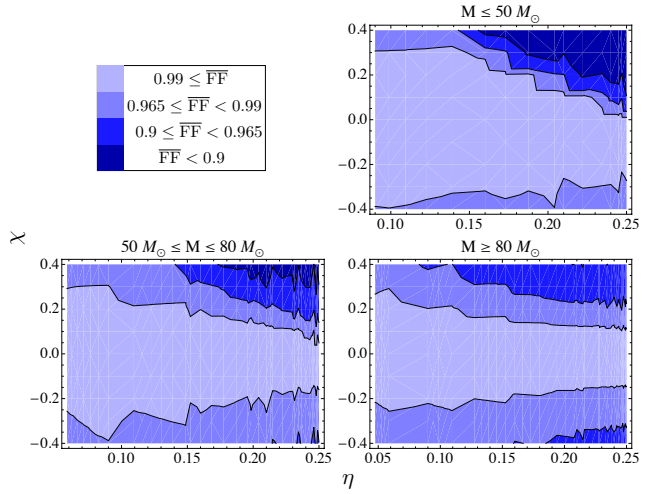

FIG. 5: Mean fitting factors ($\overline{\rm FF}$) described in the $\eta-\chi$ plane for the low-mass (top), medium-mass (bottom left), and high-mass (bottom right) systems, respectively. The mean fitting factor is calculated by averaging over M.

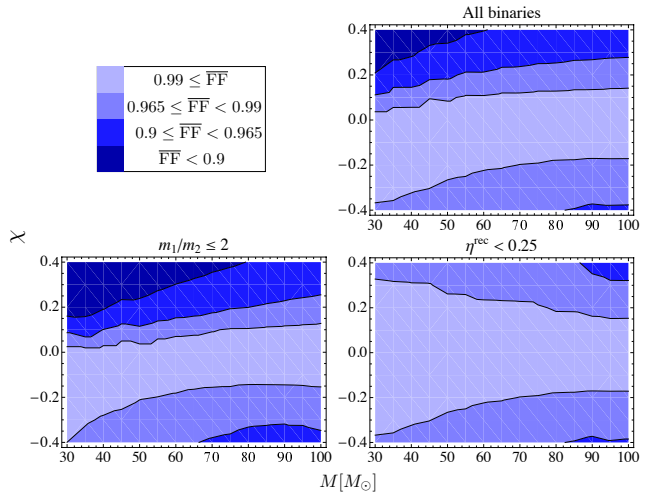

FIG. 6: Mean fitting factors ($\overline{\rm FF}$) described in the $M-\chi$ plane for all of the binaries with $M \geq 30M_\odot$ (top), symmetric-mass binaries with $m_1/m_2 \geq 2$ (bottom left), and asymmetric-mass binaries for which $\eta_{\rm rec} < 0.25$, respectively. The mean fitting factor is calculated by averaging over η.

physical boundary, and thereby the corresponding $M^{\rm rec}$ has smaller biases. We also find that the contours $\mathcal{B} = 30, -30$ in the top panels are consistent with the contours $\mathcal{B} = 15, -15$ in the bottom panels, and this indicates a linear relation between $\mathcal{B}$ and χ. Finally, we find that in the asymmetric-mass region all of the fractional biases are comparable for a given χ independently of the total mass. For example, we have $15\ (30) \lesssim \mathcal{B} \lesssim 17\ (35)$ for $\chi = -0.2\ (-0.4)$.

D. Statistical error in the parameter estimation for nonspinning BBHs

The IMC method given in Eq. (14) was established under the assumption that the posterior PDF obeys a Gaussian distribution in determining the confidence region [47]. Thus, the accuracy of this method relies on the Gaussianity of the likelihood [52], and from Eq. (13), a Gaussian likelihood corresponds to a quadratic overlap in the region given by ρ. Therefore, the confidence region obtained by the IMC method can be reliable if the overlap surface has a quadratic shape in that region. To verify this, in Fig. 9, we show the confidence region ($P = 0.99714$) and its fitting ellipse obtained by fitting a quadratic function to the overlap surface in the region of $P \geq 0.99714$. We find that the overlap contours are almost exactly overlapped with their fitting ellipses.

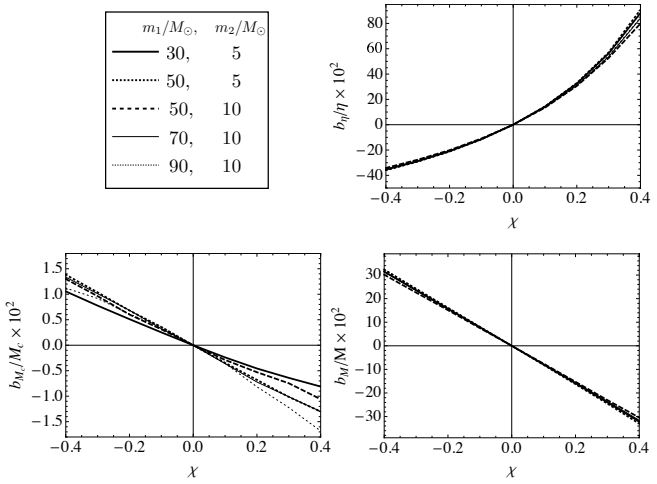

FIG. 7: Sytematic bias (b_λ/λ) as a function of χ for η (top), M_c (bottom left), and M (bottom right), respectively.

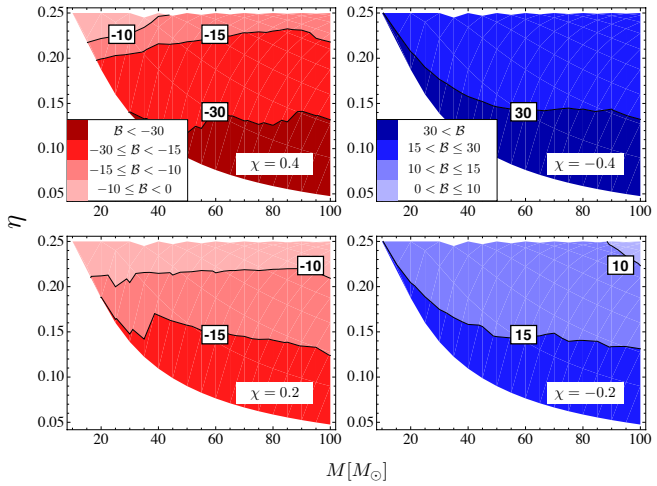

FIG. 8: Fractional biases for the parameter M ($\mathcal{B}\equiv b_M/M\times10^2$). The biases are similar between a positive (red) and a negative (blue) spins in the asymmetric-mass region ($\eta\lesssim0.15$). The similarity between the contours $\mathcal{B}=15$ (-15) and 30 (-30) indicates a linear relation between $\mathcal{B}$ and χ.

In the high SNR limit, the Fisher matrix (FM) method can be used to approximate the statistical error in the parameter estimation [53–55] (for more details refer to [56] and references therein). The FM is defined by

$$\Gamma_{ij}=\left\langle\frac{\partial\tilde{h}}{\partial\lambda_i}\middle|\frac{\partial\tilde{h}}{\partial\lambda_j}\right\rangle\Big|_{\lambda=\lambda_0}. \tag{15}$$

If the waveform model is expressed by an analytic function in the Fourier domain, the FM can be easily computed. However, unlike the post-Newtonian wave functions, the phenomenological wave functions are not so easy to apply to the FM formalism because their functional forms are much more complicated.[6]

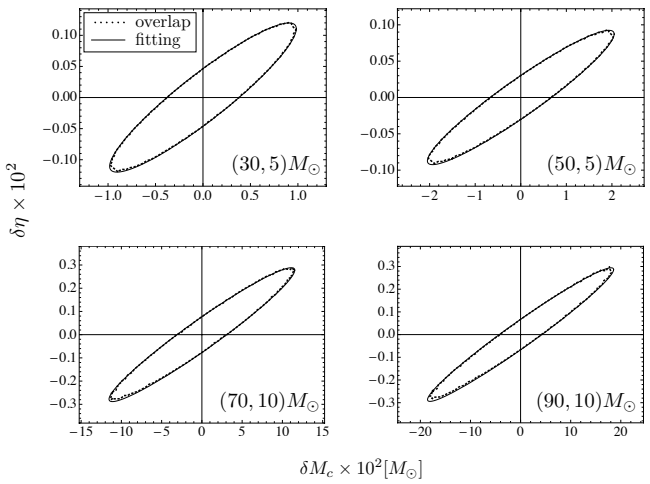

FIG. 9: One-sigma confidence region ($P=0.99714$), and its quadratic fitting ellipse. The SNR is assumed to be 20.

On the other hand, the FM can also be obtained from the log likelihood [46, 58], and the log likelihood can be approximated by the overlap as in Eq. (13). Therefore, we can calculate the FM as [46, 48, 58]

$$\Gamma_{ij}=\left\langle\frac{\partial\tilde{h}}{\partial\lambda_i}\middle|\frac{\partial\tilde{h}}{\partial\lambda_j}\right\rangle\Big|_{\lambda=\lambda_0}\simeq-\rho^2\frac{\partial^2P(\lambda)}{\partial\lambda_i\partial\lambda_j}\Big|_{\lambda=\lambda_0}. \tag{16}$$

In this work, the overlap $P(\lambda)$ is distributed in the $M_c-\eta$ space, and we showed that the overlap surface has a quadratic shape. Thus, if we find a certain analytic fitting function F to the overlap P, the derivatives in the above equation can be analytically computed. Using the function F, Cho *et al.*[46] defined the effective Fisher matrix (eFM) by

$$(\Gamma_{ij})_{\rm eff}=-\rho^2\frac{\partial^2F(\lambda)}{\partial\lambda_i\partial\lambda_j}\Big|_{\lambda=\lambda_0}. \tag{17}$$

The inverse of Γ_{ij} represents the covariance matrix of the parameter errors, and the statistical error (σ_i) of each parameter and the correlation coefficient (c_{ij}) between the two parameters are determined by

$$\sigma_i=\sqrt{(\Gamma^{-1})_{ii}},\quad \mathcal{C}_{ij}=\frac{(\Gamma^{-1})_{ij}}{\sqrt{(\Gamma^{-1})_{ii}(\Gamma^{-1})_{jj}}}. \tag{18}$$

In table I, we summarise the statistical errors calculated by using the eFM method for a nonspinning BBH system. Here,

[6] PhenomA was once applied to the FM method by Ajith and Bose [57], and Cho [42] also calculated the FM using PhenomA and PhenomC.

TABLE I: Statistical errors ($\sigma_\lambda/\lambda \times 10^2$) and correlation coefficients calculated by using the eFM method for a nonspinning BBH system with $\rho = 20$.

$m_1[M_\odot],\ m_2[M_\odot]$	30, 5	50, 5	50, 10	70, 10	90, 10
$\sigma_{M_c}/M_c \times 10^2$	0.065	0.110	0.250	0.359	0.520
$\sigma_\eta/\eta \times 10^2$	0.647	0.739	1.469	1.741	2.159
$\mathcal{C}_{M_c\eta}$	0.921	0.944	0.952	0.963	0.973
$\sigma_M/M \times 10^2$	0.329	0.341	0.648	0.705	0.798

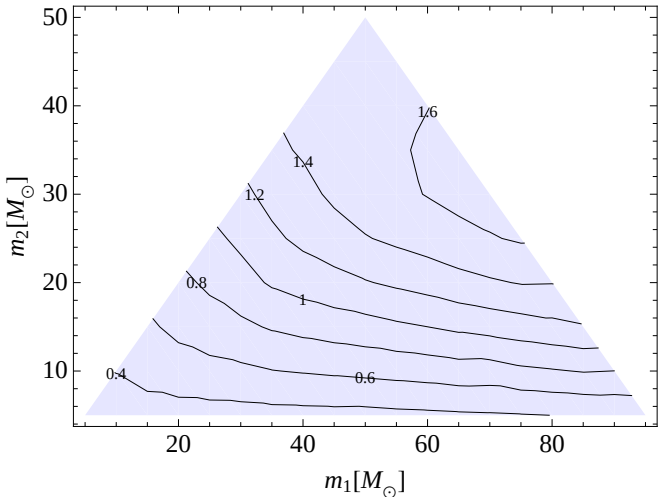

FIG. 10: Statistical errors for the parameter M. The values in the contours denote $\sigma_M/M \times 10^2$.

σ_M is computed in the following way

$$\sigma_M^2 = \left(\frac{\partial M}{\partial M_c}\right)^2 \sigma_{M_c}^2 + \left(\frac{\partial M}{\partial \eta}\right)^2 \sigma_\eta^2 + 2\mathcal{C}_{M_c\eta}\left(\frac{\partial M}{\partial M_c}\right)\left(\frac{\partial M}{\partial \eta}\right)\sigma_{M_c}\sigma_\eta, \quad (19)$$

where M is given as $M = M_c\eta^{-3/5}$. The results of the fractional error ($\sigma_M/M \times 10^2$) are given in Fig. 10 for all of the binaries. We find that the fractional errors mainly depend on the total mass in the symmetric-mass region, while in the asymmetric-mass region those strongly depend on m_2 but weakly depend on m_1. The lowest mass binary ($m_1 = m_2 = 5M_\odot$) has the minimum value of $\sigma_M/M \times 100 \simeq 0.26$, and the binary of $(70, 30)M_\odot$ has the maximum value of $\sigma_M/M \times 100 \simeq 1.69$.

E. Comparison between the statistical error and the systematic bias

Although a template bank has high fitting factors for given signals hence is believed to be efficient for the search, that can be unsuitable for the parameter estimation if the recovered parameter is significantly biased from the true parameter.

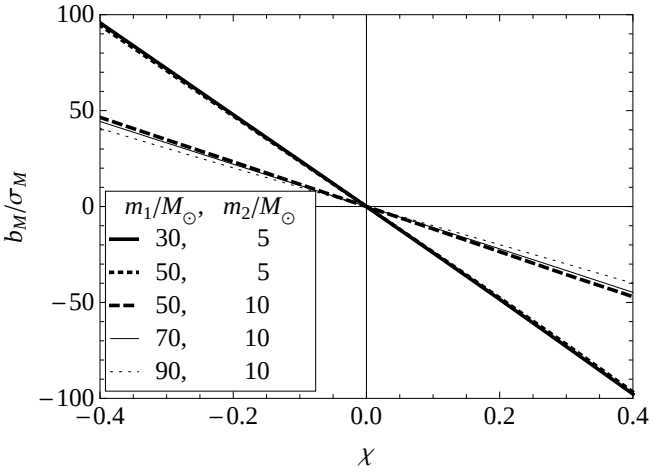

FIG. 11: Comparison between the bias and the statistical error for the parameter M.

To examine the validity of nonspinning templates for the parameter estimation for aligned-spin signals, we compare the systematic bias with the statistical error for the parameter M. The result is given in Fig. 11, where we adopt the biases and the errors given in Fig. 7 and Table I, respectively. Note that the binaries given in this result have high fitting factors in our spin range (see, Fig. 1). However, we find that the biases are much larger than the statistical errors even with a very small value of the spin. In addition, the ratio b_M/σ_M can be larger for higher SNRs because the statistical error is inversely proportional to the SNR. Therefore, we conclude that nonspinning templates are unsuitable for the parameter estimation for aligned-spin BBH signals. Interestingly, the results in this figure show clearly separated populations depending on m_2. The same tendency holds for other asymmetric-mass binaries although we show only few examples here.

IV. SUMMARY AND DISCUSSION

We investigated the efficiency of nonspinning templates in GW searches for aligned-spin BBHs. We considered the signals with moderately small spins in the range of $-0.4 \leq \chi \leq 0.4$. We employed as our waveform model PhenomD, and we set the spins to zero for the nonspinning waveforms. Using the nonspnning templates, we calculated the fitting factors of the aligned-spin BBH signals in a wide mass range up to $\sim 100M_\odot$. The results are summarised in Figs. 1 and 3 in the $m_1 - m_2$ plane and $M - \eta$ plane, respectively. The signals with negative spins can have higher fitting factors than those with positive spins. If $\chi = 0.3$, only the highly asymmetric-mass signals can have the fitting factors exceeding the threshold 0.965. However, if $\chi = -0.3$, the fitting factors for all of the signals can be larger than the threshold. The discrepancy between the regions of a positive and a negative spins is due to the fact that the template parameter space is physically restricted to $\eta \leq 0.25$ so that the recovered value of η ($\eta^{\rm rec}$) cannot exceed 0.25. We demonstrated this by choosing

the asymmetric-mass binaries that satisfy $\eta^{\rm rec} < 0.25$, and showing the nearly symmetric fitting factors for those binaries between the two regions. We classified our binaries into low-mass, medium-mass, and high-mass systems and calculated the mean fitting factor by averaging over M in the $\eta - \chi$ plane, and found that the overall area with high fitting factors is narrower for higher mass systems.

The mass parameters recovered by the nonspinning templates are significantly biased from the true parameters of the aligned-spin signals. The fractional bias (b_M/M) almost linearly depends on χ in our spin range, and all of the biases for a given χ are comparable independently of the total mass in the asymmetric-mass region ($\eta \lesssim 0.15$). On the other hand, we assessed the impact of the systematic bias (b) on the parameter estimation by comparing the bias with the statistical error (σ) assuming $\rho = 20$. We found that the ratio b_M/σ_M can exceed unity even with a very small value of the spin. We therefore confirm that nonspinning templates are unsuitable for the parameter estimation for aligned-spin BBH signals.

In actual GW search analyses, one should consider both the fitting factor and the false-alarm rate for the bank to determine the overall performance of a template bank. If one expands the nonspinning template space to three or four dimensional space by including spin parameters, the size of the bank significantly increases, and this makes the search computationally much more demanding and increases the false-alarm rate. Thus, in some cases, the search with spinning templates cannot be more sensitive to spinning signals than the same analysis using nonspinning templates due to the increase in false-alarm rate, even though the spinning templates can have higher fitting factors for the signals [59, 60]. Recently, it has been shown that the inclusion of aligned-spin effects can significantly increase the observable volume in the current Advanced LIGO search pipelines, such as **PyCBC** [26] and **GstLAL** [27]. Obviously, aligned-spin templates should be used for high-spin signals because nonspinning templates have poor fitting factors for those signals [26–28]. However, we explored the low-spin space with a nonspinning template bank, which is computationally much cheaper than an aligned-spin template bank, and showed the regions in which the aligned-spin BBH signals can achieve $\mathrm{FF} \geq 0.965$. Thus, although the current BBH searches employ aligned-spin templates [33, 34], their computational demand might be somewhat reduced by adopting nonspinning templates in the low-spin region, retaining a similar search efficiency.

ACKNOWLEDGMENTS

The author would like to thank Stephen Privitera, Tito Dal Canton, and Alex Nielsen for helpful comments. This work was supported by the National Research Foundation of Korea (NRF) grant funded by the Korea government (Ministry of Science, ICT & Future Planning) (No. 2016R1C1B2010064). This work used the computing resources at the KISTI Global Science Experimental Data Hub Center (GSDC).

[1] B.P. Abbott *et al.*(LIGO Scientific Collaboration and Virgo Collaboration), Phys. Rev. Lett. **116**, 061102 (2016).
[2] B.P. Abbott *et al.*(LIGO Scientific Collaboration and Virgo Collaboration), Phys. Rev. Lett. **116**, 241103 (2016).
[3] J. Abadie *et al.*(LIGO Scientific Collaboration), Class. Quantum Grav. **32**, 074001 (2015).
[4] F. Acernese *et al.*, Class. Quantum Grav. **32**, 024001 (2015).
[5] Y. Aso *et al.*(The KAGRA Collaboration), Phys. Rev. D **88**, 043007 (2013).
[6] J. Abadie *et al.*(LIGO Scientific Collaboration and Virgo Collaboration), Class. Quantum Grav. **27**, 173001 (2010).
[7] M. Dominik, E. Berti, R. O'Shaughnessy, I. Mandel, K. Belczynski, C. Fryer, D. Holz, T. Bulik and F. Pannarale, Astrophys. J. **806**, 263 (2015).
[8] B.P. Abbott *et al.*(LIGO Scientific Collaboration and Virgo Collaboration), arXiv:1606.03842 (2016).
[9] B.P. Abbott *et al.*(LIGO Scientific Collaboration and Virgo Collaboration), arXiv:1606.04856 (2016).
[10] B.P. Abbott *et al.*(LIGO Scientific Collaboration and Virgo Collaboration), Phys. Rev. Lett. **116**, 241102 (2016).
[11] B.P. Abbott *et al.*(LIGO Scientific Collaboration and Virgo Collaboration), arXiv:1606.01210 (2016).
[12] A. B. Nielsen, Journal of Physics: Conference Series **716**, 012002 (2016).
[13] M. Pürrer, Class. Quantum Grav. **31**, 195010 (2014).
[14] M. Pürrer, Phys. Rev. D **93**, 064041 (2016).
[15] A. Taracchini *et al.*, Phys. Rev. D **86**, 024011 (2012).
[16] A. Taracchini *et al.*, Phys. Rev. D **89**, 061502 (2014).
[17] P. Ajith *et al.*, Class. Quantum Grav. **24**, S689 (2007).
[18] P. Ajith *et al.*, Phys. Rev. D **77**, 104017 (2008); **79**, 129901(E) (2009).
[19] P. Ajith, Class. Quantum Grav. **25**, 114033 (2008).
[20] P. Ajith *et al.*, Phys. Rev. Lett. **106**, 241101 (2011).
[21] L. Santamaria *et al.*, Phys. Rev. D **82**, 064016 (2010).
[22] M. Hannam *et al.*, Phys. Rev. Lett. **113**, 151101 (2014).
[23] S. Khan *et al.*, Phys. Rev. D **93**, 044007 (2016).
[24] P. Kumar *et al.*, Phys. Rev. D **93**, 104050 (2016).
[25] P. Ajith Phys. Rev. D **84**, 084037 (2011).
[26] T. Dal Canton *et al.*, Phys. Rev. D **90**, 082004 (2014).
[27] S. Privitera *et al.*, Phys. Rev. D **89**, 024003 (2014).
[28] C. Capano, I. Harry, S. Privitera, and A. Buonanno, Phys. Rev. D **93**, 124007 (2016).
[29] I. Harry, S. Privitera, A. Bohé, and A. Buonanno, Phys. Rev. D **94**, 024012 (2016).
[30] P. Ajith, N. Fotopoulos, S. Privitera, A. Neunzert, N. Mazumder, and A. J. Weinstein, Phys. Rev. D **89**, 084041 (2014).
[31] I. W. Harry, A. H. Nitz, D. A. Brown, A. P. Lundgren, E. Ochsner, and D. Keppel, Phys. Rev. D **89**, 024010 (2014).
[32] T. Dal Canton, A. P. Lundgren, and A. B. Nielsen, Phys. Rev. D **91**, 062010 (2015).
[33] B.P. Abbott *et al.*(LIGO Scientific Collaboration and Virgo Collaboration), Phys. Rev. D **93**, 122003 (2016).
[34] B.P. Abbott *et al.*(LIGO Scientific Collaboration and Virgo Collaboration), arXiv:1606.04856 (2016).
[35] *Advanced LIGO anticipated sensitivity curves*,

https://dcc.ligo.org/LIGO-T0900288/public.
[36] T. A. Apostolatos, Phys. Rev. D **52**, 605 (1995).
[37] B. Allen, W. G. Anderson, P. R. Brady, D. A. Brown, and J. D. E. Creighton, Phys. Rev. D **85**, 122006 (2012).
[38] A. B. Nielsen, Class. Quantum Grav. **30**, 075023 (2013).
[39] J. Abadie *et al.*(LIGO Collaboration, Virgo Collaboration), Phys. Rev. D **85**, 082002 (2012).
[40] J. Aasi J *et al.*(LIGO Scientific Collaboration, Virgo Collaboration), Phys. Rev. D **87**, 022002 (2013).
[41] H.-S. Cho, Class. Quantum Grav. **32**, 215023 (2015).
[42] H.-S. Cho, Class. Quantum Grav. **32**, 235007 (2015).
[43] J. Aasi *et al.*(LIGO Scientific Collaboration, Virgo Collaboration), Phys. Rev. D **88**, 062001 (2013).
[44] L. S. Finn, Phys. Rev. D **46**, 5236 (1992).
[45] C. Cutler and E. É. Flanagan, Phys. Rev. D **49**, 2658 (1994).
[46] H.-S. Cho, E. Ochsner, R. O'Shaughnessy, C. Kim, and C.-H. Lee, Phys. Rev. D **87**, 024004 (2013).
[47] E. Baird, S. Fairhurst, M. Hannam, and P. Murphy, Phys. Rev. D **87**, 024035 (2013).
[48] H.-S. Cho and C.-H. Lee, Class. Quantum Grav. **31**, 235009 (2014).
[49] M. Boyle, D. A. Brown, and L. Pekowsky, Class. Quantum Grav. **26**, 114006 (2009).
[50] A. Lazzarini and R. Weiss, Technical document LIGOE950018-02-E (1996).
[51] M. Campanelli, C. O. Lousto, and Y. Zlochower, Phys. Rev. D **74**, 041501 (2006).
[52] C.-J. Haster, I. Mandel, and W. M. Farr, Class. Quantum Grav. **32**, 235017 (2015).
[53] H.-S. Cho, J. Korean Phys. Soc. **66**, 1637 (2015).
[54] H.-S. Cho, J. Korean Phys. Soc. **67**, 960 (2015).
[55] H.-S. Cho, arXiv:1607.07118.
[56] M. Vallisneri, Phys. Rev. D **77**, 042001 (2008).
[57] P. Ajith and S. Bose, Phys. Rev. D **79**, 084032 (2009).
[58] P. Jaranowski and A. Królak, Phys. Rev. D **49**, 1723 (1994).
[59] B. Abbott *et al.*(LIGO Scientific Collaboration), Phys. Rev. D **78**, 042002 (2008).
[60] C. Van Den Broeck *et al.*, Phys. Rev. D **80**, 024009 (2009).